Pharaoh's serpents: New insights into a classic carbon nitride material

Thomas S. Miller[a,b*], Anita d'Aleo[a], Theo Suter[a], Abil E. Aliev[a], Andrea Sella[a], Paul F. McMillan[a*]

[a] Department of Chemistry, Christopher Ingold Building, University College London, 20 Gordon Street, London, WC1H 0AJ, UK

[b] Department of Chemical Engineering, University College London, Torrington Place, London WC1E 7JE, UK.

*Email: p.f.mcmillan@ucl.ac.uk; t.miller@ucl.ac.uk

Abstract

The combustion of mercury (II) thiocyanate to form "Pharaoh's serpents" is a spectacular reaction first described nearly two centuries ago. The large volume of distinctive yellow branches that grow from a tiny quantity of flaming reactants makes this an enchanting demonstration, often used to depict the magic of chemistry. In recent years several videos of this bizarre process have "gone viral" online. Formally, the reaction should yield a carbon nitride with the ideal formula C_3N_4 along with HgS. However, since early characterization attempts there has been little further study of the materials produced. Here we apply modern characterization techniques to reinvestigate the nature of the carbon nitride and its intimate relationship to the HgS produced. This phase forms nanoparticles that decorate the internal surfaces of a matrix constituted by C_3N_4 foam. Both of these compounds are important wide-gap semiconductors and we propose that the "Pharaoh's serpents reaction" could be developed to produce a potentially useful heterojunction nanocomposite materials that could become important for optoelectronic and photocatalytic applications.

Keywords: Catalysts; Microporosity; Semiconductors; Nanoparticles; Mercury sulfide

Introduction

The discovery of novel materials often involves leaps into the unknown, either serendipitously or by design, but they can also derive from re-investigation of "classic" results from the beginnings of modern chemistry. Here we investigate one such case.

Carbon nitrides represent an emerging class of materials that are being developed for applications ranging from redox- and photo-catalysis to energy conversion and storage.[1-10] They typically have compositions within the C-N-H system, close to that of Liebig's "melon" that has an ideal structural formula $C_6N_7(NH)(NH_2)$, or C_2N_3H.[11] However, many reports

equate the materials produced with pure C_3N_4, despite the fact that this H-free formulation has only been demonstrated in a very few instances.[12, 13] This interest in producing C_3N_4 varieties was first stimulated by theoretical predictions that an sp^3-bonded framework structure might have "superhard" properties comparable to diamond,[14] but recent research has focused on graphitic layered structures based on sp^2 bonding.[13, 15-17] Interestingly, it has also been predicted that open framework varieties containing mixed sp^2 as well as sp^3 bonded units could exist.[18-21]

Most carbon nitride materials under current investigation are produced by thermolytic condensation reactions of organic molecular precursors such as dicyandiamide (DCDA, $C_2N_4H_4$) and melamine ($C_3N_3(NH_2)_3$), giving rise to a range of polymeric $C_xN_yH_z$ compounds.[22] However, Liebig's initial syntheses of 'melon' formed part of a series of studies involving reactions of thiocyanate compounds, including NH_4SCN and KSCN treated with Cl_2.[23, 24] Those investigations were initiated following Scheele's pioneering work of on prussic acid (HCN) and its salts, leading to studies of compounds containing the thiocyanate (SCN^-) anion.[25] Mercurous thiocyanate was investigated by Porret,[25] while its mercuric counterpart, $Hg(SCN)_2$, was produced by Berzelius in 1821 by reacting HgO with HSCN.[23] Based on the previous observation that cyanogen ($(CN)_2$) was formed upon heating $Hg(CN)_2$, Berzelius attempted to form analogous $(SCN)_2$ gas by heating the thiocyanate compound. However, that experiment did not give the expected result, as large quantities of CS_2 and N_2 were evolved and HgS sublimed during the highly exothermic process.[23] When the precursor was later mixed with elemental sulfur some $(SCN)_2$ was in fact produced, but the salt decomposed violently along with release of CS_2 and N_2. Interestingly, a copious quantity of a porous, pumice-like solid was also formed, this broke open the apparatus.[23] In a separate attempt to obtain thiocyanic acid (HSCN) by treating $Hg(SCN)_2$ with H_2S, Wöhler noted the characteristic snake-like appearance of the voluminous porous solid residue that emerged as the salt burned in air.[23, 26] This remarkable property led to the development of pyrotechnic materials for conjuring tricks, that were first exhibited as "Serpents du Pharaon" and later sold as "Pharaoh's serpents" eggs for personal entertainment,[26] invoking a loose reference to the mystical behavior of Moses' staff.[27] However, the observation that the demonstration caused the release of significant quantities of mercury and noxious gases into the atmosphere, as well as several instances of people confusing the wrapped pellets with ingestible sweets, or even suppositories, led to the demonstration largely falling into disuse and being replaced by other reactions that generate other solid foams of similar appearance.[23]

The overall equation for the decomposition reaction of mercury(II) thiocyanate has typically been written as:

$$2\ Hg(SCN)_2 \rightarrow 2\ HgS + CS_2 + C_3N_4 \qquad (1)$$

This equation is clearly a simplification, as the process is usually conducted in air and is accompanied by combustion of the volatile components. Nevertheless the equation implies that the reaction should result in a hydrogen-free carbon nitride, a product that is being actively sought among carbon nitride researchers.[22, 28] Franklin carried out the only reported chemical analyses of the porous yellow product in 1922, with C and N contents recorded as ranging between 35.9 – 40.2 % and 58.0 – 60.7 % by weight, respectively, with 0.6 – 2.4 wt% H present in the samples examined.[29] 39.1 wt% C and 60.9 wt% N are expected for stoichiometric C_3N_4. Solid HgS was also found to be present.[26, 29] Since that early work, no significant attention has apparently been paid to the nature of the compounds produced in the "Pharaoh's serpents" reaction. Here we present a reinvestigation of this classic carbon nitride material.

Results and Discussion

The Pharaoh's serpents reaction was initiated by igniting $Hg(SCN)_2$ on a flame-proof mat. The dried material was pressed into a pellet before it was ignited in a fume hood (essential) using a propane torch (Figure 1 and see also movie M1 in Supporting Information). As the reaction began, yellow/brown columns of solid material (which sometimes branch) immediately began to emerge from the flaming pellet (Figure 1b, c), while some black material could also be observed near the base of the emerging branches. The reaction is observed to be substantially exothermic and self-propagating, continuing until the starting material is exhausted.

A striking feature of the reaction is the huge volume expansion that takes place as the product (which we will refer to as "Pharaoh's serpent" or "serpents" for convenience) forms. The "serpents" are extremely light and fragile suggesting that the material is a blown foam that forms through a polymerization process accompanied by the release of large volumes of gas that cause expansion of the solid phase. The initial gaseous product is thought to be predominantly carbon disulfide, which boils at 46 °C.[30] The reaction is accompanied by blue flames observed around the bottom few centimeters of the growing column of material. This is consistent with the evolved CS_2 burning in air to produce SO_2 and CO_2, that contribute to the expansion. The flame color is characteristic of burning elemental sulfur and S-rich

substances in air, and it has been attributed to the continuum emission from electronically excited SO[31] as well as to a triplet to single transition in excited SO_2.[31, 32] The strongly exothermic combustion of CS_2 (ΔH = –1075 kJ/mol)[30] likely contributes to the self-propagating character of the reaction.

To explore further the role of CS_2 in the combustion process we conducted the Pharaoh's serpents reaction under a nitrogen environment, using an electrically heated glowing Nichrome wire to ignite the pellet. The reaction commences similarly to that observed in air, and once more causes formation of the distinctive expanded solid product (see movie M2 in Supporting Information). However, under these conditions the reaction did not continue to completion, indicating that the exothermic combustion of CS_2 in the presence of oxygen does indeed serve to sustain the thiocyanate decomposition reaction.

Examination of the reaction products in air showed that the Pharaoh's serpent branches were distinctly yellow on the outside, but when broken open it could be seen that these surrounded a black-gray colored core (Figure 1c, inset). We assert that the dark color is due to the presence of HgS, which is removed from the outer part of the column by the heat of the combustion reaction, leaving the characteristic yellow color common to many carbon nitrides.[22]

$$HgS + O_2 \rightarrow Hg + SO_2 \qquad (2)$$

Consistent with this interpretation, the reaction in a nitrogen atmosphere yielded a significantly grayer colored product.

Due to the mechanical fragility of the serpent foam it was not possible to reliably separate the yellow outer material from the darker core with confidence. Combustion analysis of the overall bulk showed that the light element (CNH) composition of the material was: C 38.1 (±0.1) wt%, N 59.9 (± 0.3) wt%; and H 2.0 (± 0.2) wt%, in good agreement with the values reported by Franklin.[29] Importantly, these values result in a C/N ratio (0.742) that is very close to the ideal C_3N_4 stoichiometry (0.75), as expected from the chemical equation (1) above. Elemental analysis of the Pharaoh's serpent material produced in an N_2 atmosphere showed a similar C/N ratio but here the products were expected to be affected by incomplete combustion and removal of the CS_2 and HgS components from the reaction mixture.

The H content determined by bulk chemical analysis could be due to N-H groups present within the material through interaction with atmospheric moisture during combustion in air, or to H_2O adsorbed on the surface of the highly porous samples produced by the synthesis reaction. These considerations both affect and are partly resolved by our IR, ^{13}C and ^{15}N NMR spectroscopic observations that are discussed below.

Thermogravimetric analysis (TGA) conducted in helium (Figure 2a) shows two significant mass loss events. The first and major loss (78.5 wt %) that occurs between 245 – 370 °C can be assigned to HgS decomposition and removal. A sulfur analysis found 11.8 wt % sulfur in the serpents produced in air. If a 1:1 S to Hg ratio is assumed, this equates to 80 wt % HgS present in the Pharaoh's serpent material, consistent with the mass loss recorded in the TGA data. Interestingly, the temperature range recorded for HgS decomposition is very low: this feature is discussed below.[33, 34] The second mass loss event, occurring between 370 and 500 °C (16.5 wt %) is characteristic of thermal degradation of the carbon nitride and is consistent with the total wt % of the C_3N_4 (18.7 wt %) component found from elemental analysis.

We investigated the local structure and atomic environments within the C_3N_4 component of the Pharaoh's serpent material using X-ray photoelectron spectroscopy (XPS), solid state magic angle spinning (MAS) ^{13}C and ^{15}N NMR, IR and Raman spectroscopy techniques.

XPS data from the C1s and N1s regions of the material provide further information on the local atomic structural environments as well as the chemical composition (Figure 2 b, c, Figure S1). The C1s peak at 284.8 eV is assigned to C-C bonds commonly present in "adventitious" carbon (C_{adv}) species and is disregarded. The dominant peak at 288.2 eV is consistent with sp^2 C atoms bonded to N within either triazine or heptazine ring units.[22] The shoulder on this peak at slightly lower binding energy (BE) indicates a third feature at 286.7 eV.[22] This could be assigned to a small amount of terminal sp-bonded carbon atoms occurring within C≡N groups, as suggested to be present by IR spectroscopy (see below). The XPS data indicate that the very small quantity of O detected can be attributed to adventitious species derived from interaction with the atmosphere during or subsequent to the synthesis reaction (Figure S2).

The N1s spectrum (Figure 2c) is dominated by a strong peak at 398.2 eV due to sp^2 bonded C-N=C nitrogen environments.[22] A shoulder appears at higher BE (400.6 eV), in a position similar to that observed in H-free potassium cyamelurate (KCM: $C_6N_7O_3K_3$) and

triphenylamine.[22] Because of the low H content of the Pharaoh's serpent determined by analysis and shown by IR spectroscopy (see below) we suggest that this contribution can be assigned to the sp^2 N-C_3 species that appear either at the center of heptazine (C_6N_7) rings or as bridging units between independent C_3N_3 rings in condensed triazine-based graphitic-C_3N_4 structures. This peak cannot reliably be deconvoluted further, but we cannot rule out that could also contain some contribution from N-H containing defects included within the bulk material. Excluding the C_{adv} component, the C:N atomic ratio is found to be either 3.1:4 or 2.6:4, depending on whether or not the 286.7 eV C1s peak is included in the discussion. However, from our analysis of the XPS data we can conclude that the chemical composition of the yellow-brown matrix material is indeed close to the ideal formula C_3N_4.

We next discuss the interpretation of the IR and Raman spectroscopic data. Kouvetakis et al reported an IR spectrum for nanocrystalline g-C_3N_4 prepared by chemical vapor deposition. A broad absorption band was observed extending between 1150 - 1650 cm^{-1}, with absorption maxima visible near 1250, 1340, 1550 and 1630 cm^{-1}.[12] Thin flakes of triazine-based graphitic carbon nitride (TGCN) exhibit similar spectra but with a greater number of maxima visible.[13] In particular, two features at 1620 and 1570 cm^{-1} appear as distinct bands, whereas a sharp peak occurs at 805 cm^{-1}. These IR absorptions can be assigned to in-plane C-N stretching and NCN/CNC bending vibrations of the sp^2-bonded structure. In both studies a weak feature appeared near 2300 cm^{-1} due to terminal -C≡N stretching vibrations. Our spectra for the Pharoah's serpent compound are similar with a main absorption band extending between 1050-1450 cm^{-1} containing maxima at 1070, 1157, 1205, 1243, 1300 and 1397 cm^{-1}, and a lower intensity band at 1590 cm^{-1}. There is also a sharp peak near 800 cm^{-1}, along with very weak features in the 1900 - 2300 cm^{-1} region (Fig. 2). Unfortunately we cannot use the appearance of the IR spectra to distinguish between the possible presence of triazine- *vs* heptazine-based structures.[22] The comparison with triazine-based g-C_3N_4 materials is described above. The obvious feature at 1590 cm^{-1} is similar to a band found for N-H free alkali cyamelurates ($C_6N_7O_3R_3$, R=Cs, Rb, K, Na, Li), that have structures based on heptazine units.[35] However, crystalline compounds based on a polytriazine imide (PTI) layered motif such as PTI·LiCl, PTI·LiBr or $C_6N_9H_3$·HCl also contain a similar feature at around the same position.[22, 36] That feature has been mainly associated with N-H bending vibrations in these compounds, as has also been discussed for polymeric $C_xN_yH_z$ materials related to Liebig's melon[22] (Fig. 2), but absorption maxima near this position have also been recorded for the nominally H-free nanocrystalline g-C_3N_4 and TGCN samples.[12, 13] The IR data provide useful information on the likely H content of the Pharaoh's serpent compound.

In Figure 2d we compare a typical spectrum with that of a polymeric $C_xN_yH_z$ material prepared by heating melamine to 550 ^oC. That compound has a structure related to Liebig's melon based on linked polyheptazine chains containing -NH- and -NH_2 groups and it was determined to contain 1.4 wt% H. The strong band between approximately 2900 - 3400 cm^{-1} is assigned to N-H stretching vibrations. Although a weak feature is present in this region for the Pharaoh's serpent material, its intensity is considerably lower suggesting that the number of N-H bonds is significantly less.

Raman spectra were obtained for the porous C_3N_4 matrix produced by the Pharaoh's serpent reaction using UV (325 nm) laser excitation (Figure 2e). We note that the material exhibits a significantly stronger photoluminescent background than other graphitic-polymeric $C_xN_yH_z$ or PTI-based compounds when excited with short wavelength radiation.[22] The strong fluorescence signal precluded observation of the weak Raman bands using other visible wavelengths. It has been argued that the UV excitation results in observation of highly localized structures within the amorphous material due to a combination of electronic and optical effects.[37] The overall form of the spectrum is similar to that observed for the polymeric $C_xN_yH_z$ compound that has a heptazine-based structure. However, the distinctive features at 980 and 690 cm^{-1} have also been associated with symmetric stretching motions of independent C_3N_3 rings within polytriazine imide structures.[37, 38]

We carried out further investigations of the structure of the carbon nitride material using ^{13}C and ^{15}N NMR spectroscopy (Figure 3). It is important to note that although the H content within the material is low, the protons attached within N-H bonds can be used to obtain cross-polarization (CP) information on the ^{13}C and ^{15}N sites. The ^{13}C NMR CP-MAS spectra with TOSS (total suppression of spinning sidebands) reveal two peaks at approximately 156 and 164 ppm confirming the presence of sp^2 hybridised carbons (Figure 3a).[11, 39] There was no indication of sp^3 carbon. A spectrum acquired using the NQS (non-quaternary suppression) technique (Figure 3a) showed no significant intensity loss for either of the peaks suggesting that both peaks are due to quaternary carbon atoms with no protons directly attached to them, consistent with the IR data. Although the peak heights are different, the asymmetric peak with its maximum at 156 ppm is broader than the peak at 164 ppm and it may contain two unresolved components. An iterative deconvolution of the spectrum using mixed Lorentzian (40%) - Gaussian (60%) lineshapes (Figure 3b, c) suggests that the use of 3 peaks at 163.9, 156.0 and 151.0 ppm is sufficient to reproduce the observed asymmetry in the low-frequency region (Figure 3c). The observed asymmetry in

the lineshape of the low-frequency peak could be due to a number of reasons, including structural inhomogeneity as well as the effect of ^{13}C,^{14}N residual dipolar couplings, that are known to be significant at a relatively low magnetic field of 7.05 T.[40]

In their study of triazine based graphitic C_3N_4 (TGCN), Algara-Siller *et al.* observed a broad resonance spanning a similar range (145 - 172 ppm with a maximum near 160 ppm) to that observed for the Pharaoh's serpent material.[13] (Figure S3). Although their sample was nominally H-free, both CP-MAS ^{1}H-^{13}C and ^{1}H-^{15}N spectra were reported in their study. From comparison of lineshapes in the single-pulse and CP-MAS spectra of TGCN, it is apparent that there are at least two overlapping signals, with peak maxima occurring between 155-165 ppm. In their study of the polytriazine imide (PTI) structured compound $C_6N_9H_3{\cdot}HCl$, containing triazine rings linked by -NH- groups, Zhang *et al.* used both single-pulse and CP-MAS techniques to observe two peaks at 166 and 159 ppm with similar relative intensities (Figure S4),[36] similar to those observed for the Pharaoh's serpent. The related crystalline compound PTI·LiCl also showed three peaks at 168, 162.6 and 157.9 ppm with relative intensities that evolved as a function of CP-MAS NMR contact times.[41] The resonances at 162.6 and 157.9 ppm showed a rapid CP build up and could be assigned to ^{13}C environments close to the bridging -NH- groups, whereas the peak at 168 ppm was attributed to C atoms adjacent to nonprotonated N atoms. Three peaks at 167.9, 162.6 and 157.8 ppm were also observed for PTI·LiBr with CP dynamics similar to those in PTI·LiCl,[42] although the intensity of the 157.8 ppm peak was significantly smaller than the other two in the single-pulse ^{13}C MAS NMR spectrum. These observations might suggest that the Pharaoh's serpent material has a structure based on triazine (C_3N_3) rings linked *via* bridging -N=, along with some -NH- units, as found in the g-C_3N_4, TGCN and PTI structures, with the possibility that some three-dimensional linking might occur to form polymeric units as predicted by theoretical studies.[18, 19, 21]

However, the ^{13}C chemical shifts observed for our Pharaoh's serpent materials also match closely with those observed for structures based on linked heptazine (tri-s-triazine, C_6N_7) units, including Liebig's *melon*, *melem* (triamino-s-heptazine) and other substituted molecular heptazine complexes.[11, 39, 43, 44] Lotsch *et al.*[11] reported two signal groups with peak maxima at 164 and 157 ppm for Liebig's melon.[11] (Figure S5). Jürgens *et al.* found a strong peak at 155.1 ppm with a shoulder at 156 ppm for melem that was comparable with signals found for $C_6N_7H_3$ and $C_6N_7Cl_3$.[39] This was assigned to C_iN_3 atoms of the cyameluric nucleus. Two peaks at 164.3 and 166.4 ppm were assigned to C_e atoms adjacent to the NH_2

groups of the melem structure.[39] Hu *et al.* reported two peaks with equal integral intensity at 164 and 157 ppm in the single-pulse ^{13}C MAS NMR spectrum of graphitic carbon nitrides prepared from ^{13}C,$^{15}N_2$-labelled urea.[45] The integral intensity ratio was found to change to 2 (164 ppm) : 1 (157 ppm) in the CP-MAS spectrum. We can conclude that significantly different structural models have been advanced to interpret the structures of these various materials that exhibit quite similar ^{13}C NMR spectra.[11, 13, 36, 45] For example, Algara-Siller *et al.* based their NMR interpretation on a triazine-based g-C_3N_4 structure,[13] whereas Lotsch *et al*.[11] and Hu *et al.*[45] explained their NMR data using the heptazine-based Liebig's melon structure, and Zhang *et al.*[36] attributed their data to a PTI layered compound.

We then conducted an acquisition of the ^{15}N CP-MAS spectrum of the Pharaoh's serpent material. Because the main component is HgS, as found by elemental analysis, while only 18.7 wt % is C_3N_4, the ^{15}N NMR experiment faced severe problems for data acquisition due to the low sensitivity of the ^{15}N nucleus in its natural abundance. Within the carbon nitride samples, the small (<2%) H content further complicated data acquisition and interpretation during the ^{15}N CP-MAS experiment, that relies on $^{1}H \rightarrow {}^{15}N$ cross-polarisation. The result of a two-week long spectral acquisition is shown in Figure 3d. Two distinct regions of ^{15}N NMR signals can be identified. The signals in the high-frequency region between -170 and -200 ppm (210 and 180 ppm relative to $MeNO_2$) are assigned to cyclic nitrogen atoms with no directly attached protons. The signals in the low-frequency region between -210 and -290 ppm (170 and 90 ppm relative to $MeNO_2$) are typically assigned to protonated nitrogens of NH and NH_2 groups.[11, 39] Given that these are spectra recorded under cross-polarisation conditions, this implies that the "quaternary" nitrogens (those not bonded to hydrogen) are significantly more abundant than the NH sites, consistent with the infrared spectra.

We can compare our ^{15}N CP-MAS spectrum with those reported by Algara-Siller *et al.*[13](Figure S6) and Lotsch *et al*.[11] (Figure S7), that resemble more closely the ^{15}N CP-MAS measured for the Pharaoh's serpent material than those of PTI·LiCl,[41] PTI·LiBr[42] or PTI·HBr.[37] We note that a ^{15}N-labelled Liebig's melon was used in the ^{15}N NMR measurement by Lotsch *et al*.[11] that allowed unambiguous identification of the small signal at approximately –225 ppm (156 ppm relative to $MeNO_2$) due to the central heptazine N_c atom that is diagnostic of the heptazine structural unit. Our data recorded at the natural abundance level do not allow us to draw firm conclusions regarding the presence or absence of this type of site. The observation of this key N_c atom is further complicated by the fact that it is distant from any protons present in -NH- linked units, resulting in poor $^{1}H \rightarrow {}^{15}N$

efficiency in CP-MAS spectra compared to other nitrogen atoms. This conclusion is supported by our measurement of the natural-abundance ^{15}N CP-MAS spectrum of a Liebig's melon sample using a short contact time of 1 ms, that shows a considerable attenuation of the signal intensity at -224 ppm (Figure S8). The ^{15}N CP-MAS spectrum reported by Lotsch *et al.* for a similar sample was recorded using a contact time of either 10 or 20 ms.[11] Overall, our ^{15}N CP-MAS NMR spectrum confirms the presence of H atoms directly attached to N atoms in the form of NH and NH_2 groups. As can be seen from comparison of the spectra shown in Figures S6 and S7, the ^{15}N CP-MAS spectrum of Pharaoh's serpent material resemble that of TGCN[13] more closely than that of Liebig's melon.[11]

Our conclusion from the spectroscopic analysis of the Pharaoh's serpent C_3N_4 material is that it is based on sp^2 bonded C atoms within triazine or *s*-heptazine ring units, or a mixture of both species, linked together by bridging N atoms.

Scanning electron microscope (SEM) images of the Pharaoh's serpent clearly show the highly porous nature of the Pharaoh's serpent carbon nitride foam (Figure 4a). This structure is likely to derive from the large volumes of gas released during synthesis, combined with the mechanical flexibility of the interconnected C_3N_4 structural motifs.[18, 46] Interestingly it appears to consist of extended, sheet-like layers that are folded and twisted to leave micron-sized voids. Point spectra from energy-dispersive X-ray spectroscopy (EDS) confirm the presence of Hg and S in a ratio close to 1:1 throughout the structures.

Although the SEM-EDS analysis clearly indicate the presence of HgS across the sample, only a small number of particles with a cubic or spherical morphology could be observed in the images obtained (Figure S9). However, we note that the surfaces of the carbon nitride sheets also present a "mottled" appearance due to features on a smaller length scale. To investigate this further, transmission electron microscope (TEM) images were taken (Figure 4b and Figure S10). It is immediately apparent from these images that the carbon nitride sheets are coated by a filigree pattern of discrete HgS nanoparticles with diameters ranging between ~5 and 10 nm (Figure 4b). These can be seen to cluster together, forming extended dendritic structures. EDS mapping of a section of Pharaoh's serpent suspended above the void in the holey carbon grid confirms that C and N are consistently observed across the whole backbone structure, showing that the underlying support material is indeed the carbon nitride matrix (Figure 4c - f). However, Hg and S are limited to those areas where the

nanoparticle dendrite assemblies are observed. This HgS nanoparticle deposition was found consistently across the vast majority of the surface (Figure 4b and Figure S10), although some areas were found to be free from metal sulfide particles (Figure S10), indicating that they are distinct from the carbon nitride matrix component. This result is particularly interesting as HgS nanoparticles have been identified as semiconductors with potentially useful luminescent and photocatalytic properties that are complementary to those of the carbon nitride itself.[8, 47] Previous attempts to create HgS nanoparticles within a specified size range below ~10 nm have involved complex and time-consuming processes including chemical vapor deposition (CVD) or hydrothermal synthesis.[47-49] The classic "Pharaoh's serpent" synthesis approach could yield large quantities of HgS nanoparticles decorating the porous C_3N_4 matrix material. The nanoscale dimensions of the HgS particles is likely to lead to a depression of the decomposition temperature, as is commonly found for nanomaterials, which is consistent with our TGA results.

TEM images of the HgS particles (Figure 5a) indicated their crystallinity and fast Fourier transform (FFT) suggested a cubic lattice,[30] consistent with the black β-HgS (metacinnabar) form. The red α-HgS polymorph has a trigonal lattice.[30] Selected area electron diffraction (SEAD) patterns taken from clusters of HgS particles (Figure 5b) show series of concentric rings constructed from a multiple points, indicating collections of randomly orientated crystals. The first ring corresponds to a *d* spacing 3.0 nm^{-1} and is assigned to the 111 plane (calc. 2.96 nm^{-1}) using the characteristic unit cell length (*a*) of β-HgS (5.85 Å).[30] The second (*d* = 4.9 nm^{-1}, calc. 4.83 nm^{-1}) and third (*d* = 5.8 nm^{-1}, calc. 5.92 nm^{-1}) rings are assigned to 202 and 222 planes, respectively. An expected weak ring for the 200 plane calculated at *d* = 3.4 nm^{-1} was not detected, perhaps suggesting some preferred orientation effects. Powder X-ray diffraction (pXRD) data from the Pharaoh's serpent material confirms the assignment of the β-HgS polymorph (Figure 5c). Reflections from the carbon nitride phase are not visible due to its low crystallinity and the comparatively low scattering power of the light C and N atoms.

The XPS data in the Hg 4f and S 2p regions of the spectra (Figure 5d and e respectively) agree with the expected stoichiometry (Hg:S atomic ratio determined as 1:1). Both regions can be fitted by two Gaussian-Lorentzian (GL) peaks, indicating a single bonding environment in each case according to spin-orbit coupling relationships (I = $^1/_2$, $^3/_2$ for S2p and $^5/_2$, $^7/_2$ for Hg4f). There was no evidence for metallic Hg (binding energy = 99.8 eV), indicating that any

metallic Hg produced was vaporized during the self-propagating high-temperature synthesis (SHS).

Conclusions

We have shown that the classic demonstration experiment involving thermally initiated decomposition of $Hg(SCN)_2$ to form "Pharaoh's serpents" results in formation of a potentially useful nanocomposite semiconductor material consisting of nano-HgS decorating the surfaces of a porous C_3N_4 matrix with a composition close to C_3N_4. NMR, FTIR, XPS and Raman results suggest that the carbon nitride material may be based either on linked heptazine or triazine units, or a combination of both. Although previous studies on carbon nitride systems would lead one to expect the structure to be layered, we cannot rule out the possible existence of three-dimensional framework components as suggested by theoretical calculations.[18, 19, 21] The formation reaction and presence of Hg in the resulting nanocomposite may hinder the practical implementation of these materials but related synthesis pathways can now be envisaged to create analogous semiconductor heterojunction combinations using more environmentally friendly elements. Analysis of this "classical" reaction and its products could give rise to more readily scalable ways to produce such nanoscale materials composites with useful properties for energy and sustainability applications.

Experimental

Making Pharaoh's serpent: Approximately 2 g of mercury (II) thiocyanate (Sigma-Aldrich, 96.5 %) was compacted into a pellet using a 1 cm pellet press (2000 psi) and ignited in a fume hood using a propane torch. A movie of this process can be seen in supporting information (movie M1). **CAUTION STATEMENT: This reaction emits mercury vapor and other hazardous gases. Always use extraction for this experiment.**

Making Pharaoh's serpent under N_2: Approximately 2 g of mercury (II) thiocyanate (Sigma-Aldrich, 96.5 %) was compacted into a pellet using a 1 cm pellet press (2000 psi). A hole was then drilled through this pellet and it was suspended from a nichrome wire. This was used to suspend the pellet within a glass bottle, which was thoroughly purged with N_2. An electrical current (~1.5 A) was passed through the wire to induce resistive heating, this ignited the pellet. A movie of this process can be seen in supporting information (movie M2). **CAUTION STATEMENT: This reaction emits mercury vapor and other hazardous gases. Always use extraction for this experiment.**

Making polymeric CxNyHz: Melamine (~1.5 g, 99%, Sigma-Aldrich) was ground then packed into an alumina boat. The boat was then heated under flowing N_2 at 10 °C min^{-1} to 550 °C in a tube furnace (Carbolite, MTF 12/38/250) and held for 6 h, before being cooled to room temperature.

Characterization: Elemental analysis was carried out at the using a Vario MICRO cube elemental analyzer (Elementar). TGA was run on a Netszch TGA instrument. The material was loaded into an alumina crucible (~5 mg), which was heated under He at 5 ˚C/min from room temperature to 750 ˚C. High-resolution solid-state ^{13}C were recorded on a Bruker Avance 300 spectrometer with 7.05 T wide-bore magnet at ambient probe temperature and at 75.5 MHz using a Bruker 4 mm double-resonance magic-angle spinning (MAS) probe and zirconia rotors spun at the MAS frequency of 8 kHz with stability better than ±3 Hz. Typical acquisition conditions for ^{13}C CP-MAS TOSS experiments were: ^{1}H 90° pulse duration = 2.45 µs; contact time = 2 ms; recycle delay = 5 s. Dipolar-dephased (NQS) ^{13}C CP-MAS TOSS spectra were also acquired with a dephasing delay of 40 µs. ^{13}C NMR chemical shifts are given relative to tetramethylsilane, calibrated using glycine (176.46 ppm). Typical acquisition conditions for ^{15}N CP-MAS experiments were: ^{1}H 90° pulse duration = 2.45 µs; contact time = 2 ms; recycle delay = 5 s. ^{15}N NMR chemical shifts are given relative to nitromethane, calibrated using glycine (-347.2 ppm). XPS measurements were performed using a Thermo Scientific Kα spectrometer, using monochromated Al Kα. Radiation. FE-SEM images were taken using a JEOL JSM-6700F system. Images of bulk PTI powders were taken of ground samples which were dropped onto conductive carbon tape. TEM images were taken using a JEOL JEM-2100 TEM (accelerating voltage of 200 kV). Samples were prepared by sonicating the Pharaoh's serpent in methanol and dropping the suspension onto holey carbon TEM grids (Cu 300 mesh, Elektron Technology UK ltd). IR spectra were acquired using an attenuated total reflectance (ATR) FTIR (IRTracer-100, Shimadzu). Micro-Raman spectra were taken using a Renishaw InVia spectrometer fitted with a 325 nm UV laser. XRD patterns were taken on a Stoe Stadi-P (Cu) Capillary Power XRD with a Kα1 radiation source using borosilicate glass capillaries (OD 0.5 mm, capillary tube supplies ltd).

Elemental analysis (duplicate, wt %). Pharaoh's serpent produced in air: C 7.13, 7.06; H 0.42, 0.34; N 11.14, 11.17; S 11.84, 11.81. Pharaoh's serpent produced in N_2: C 6.30, 6.24; H 0.59, below limit of detection (0.3 %); N 9.58, 9.47; S 13.87, 13.40.

Acknowledgements

This project has received funding from the European Union's Graphene Flagship under Horizon 2020 research and innovation programme grant agreement No. 696656 – GrapheneCore1 and from the EPSRC EP/L017091/1. The authors would also like to thank Dr Chris Howard and Dr Patrick Cullen for their help with photography and electron diffraction analysis and Mr Emre Sener for assistance with the electrical ignition experiments.

References

[1] A. B. Jorge Sobrido, I. Dedigama, N. Mansor, R. Jervis, T. S. Miller, F. Corà, P. Shearing, C. Gibbs, P. F. McMillan, D. J. Brett, *ECS Trans.* **2015**, *64*, 13-30.

[2] N. Mansor, T. S. Miller, I. Dedigama, A. B. Jorge, J. Jia, V. Brázdová, C. Mattevi, C. Gibbs, D. Hodgson, P. R. Shearing, C. A. Howard, F. Corà, M. Shaffer, D. J. L. Brett, P. F. McMillan, *Electrochim. Acta* **2016**, *222*, 44-57.

[3] T. S. Miller, A. B. Jorge, A. Sella, F. Corà, P. R. Shearing, D. J. L. Brett, P. F. McMillan, *Electroanalysis* **2015**, *27*, 2614-2619.

[4] M. Wu, Q. Wang, Q. Sun, P. Jena, *J. Phys. Chem. C* **2013**, *117*, 6055-6059.

[5] A. Thomas, A. Fischer, F. Goettmann, M. Antonietti, J. O. Muller, R. Schlogl, J. M. Carlsson, *J. Mater. Chem.* **2008**, *18*, 4893-4908.

[6] J. Liu, Y. Liu, N. Liu, Y. Han, X. Zhang, H. Huang, Y. Lifshitz, S. T. Lee, J. Zhong, Z. Kang, *Science* **2015**, *347*, 970-974.

[7] V. W. H. Lau, I. Moudrakovski, T. Botari, S. Weinberger, M. B. Mesch, V. Duppel, J. Senker, V. Blum, B. V. Lotsch, *Nat. Commun.* **2016**, *7*, 12165.

[8] W. J. Ong, L. L. Tan, Y. H. Ng, S. T. Yong, S. P. Chai, *Chem. Rev.* **2016**, *116*, 7159-7329.

[9] H. Ou, L. Lin, Y. Zheng, P. Yang, Y. Fang, X. Wang, *Adv. Mater.* **2017**, 1700008.

[10] L. Lin, H. Ou, Y. Zhang, X. Wang, *ACS Catal.* **2016**, *6*, 3921-3931.

[11] B. V. Lotsch, M. Döblinger, J. Sehnert, L. Seyfarth, J. Senker, O. Oeckler, W. Schnick, *Chem. Eur. J.* **2007**, *13*, 4969-4980.

[12] J. Kouvetakis, M. Todd, B. Wilkens, A. Bandari, N. Cave, *Chem. Mater.* **1994**, *6*, 811-814.

[13] G. Algara-Siller, N. Severin, S. Y. Chong, T. Björkman, R. G. Palgrave, A. Laybourn, M. Antonietti, Y. Z. Khimyak, A. V. Krasheninnikov, J. P. Rabe, U. Kaiser, A. I. Cooper, A. Thomas, M. J. Bojdys, *Angew. Chem. Int. Ed.* **2014**, *53*, 7450-7455.

[14] A. Y. Liu, M. L. Cohen, *Science* **1989**, *245*, 841.

[15] E. Kroke, M. Schwarz, *Coord. Chem. Rev.* **2004**, *248*, 493-532.

[16] T. S. Miller, T. M. Suter, A. M. Telford, L. Picco, O. D. Payton, F. Russell-Pavier, P. L. Cullen, A. Sella, M. S. P. Shaffer, J. Nelson, V. Tileli, P. F. McMillan, C. A. Howard, *Nano Lett.* **2017**.

[17] A. I. Cooper, M. J. Bojdys, *Mater. Today* **2014**, *17*, 468-469.

[18] C. J. Pickard, A. Salamat, M. J. Bojdys, R. J. Needs, P. F. McMillan, *Phys. Rev. B* **2016**, *94*, 094104.

[19] D. T. Vodak, K. Kim, L. Iordanidis, P. G. Rasmussen, A. J. Matzger, O. M. Yaghi, *Chem. Eur. J.* **2003**, *9*, 4197-4201.

[20] A. Salamat, M. Deifallah, R. Q. Cabrera, F. Corà, P. F. McMillan, *Sci. Rep.* **2013**, *3*, 2122.
[21] H. Dong, A. R. Oganov, Q. Zhu, G. R. Qian, *Sci. Rep.* **2015**, *5*, 9870.
[22] T. S. Miller, A. B. Jorge, T. M. Suter, A. Sella, F. Cora, P. F. McMillan, *Phys. Chem. Chem. Phys.* **2017**, *19*, 15613-15638.
[23] H. Irving, *Sci. Prog.* **1935**, *30*, 62-66.
[24] J. V. Liebig, *Ann. Pharm. (Lemgo Ger.)* **1834**, *10*, 10.
[25] R. Porrett, *Philos. Trans. R. Soc. London* **1814**, *104*, 527-556.
[26] T. L. Davis, *J. Chem. Educ.* **1940**, *17*, 268.
[27] The Holy Bible: King James edition, Exodus vii, 8-12.
[28] F. K. Kessler, Y. Zheng, D. Schwarz, C. Merschjann, W. Schnick, X. Wang, M. J. Bojdys, *Nat. Rev. Mater.* **2017**, *2*, 17030.
[29] E. C. Franklin, *J. Am. Chem. Soc.* **1922**, *44*, 486-509.
[30] W. M. Haynes, D. R. Lide, *CRC handbook of chemistry and physics : a ready-reference book of chemical and physical data*, CRC Press, Boca Raton, **2011**.
[31] C. J. Halstead, B. A. Thrush, *Proc. R. Soc. A* **1966**, *295*, 380.
[32] G. Herzberg, *Molecular Spectra & Molecular Structure III (Polyatomic Molecules)*, Van Nostrand, New York, **1966**.
[33] P. Baláž, J. Briančin, V. Šepelák, I. Hocmanová, *Thermochim. Acta* **1992**, *196*, 349-355.
[34] M. Földvári, *Handbook of Thermogravimetric System of Minerals and Its Use in Geological Practice*, Geological Institute of Hungary (Magyar Állami Földtani Intézet), **2011**.
[35] E. Horvath-Bordon, E. Kroke, I. Svoboda, Fue, R. Riedel, S. Neeraj, A. K. Cheetham, *Dalton Trans.* **2004**, 3900-3908.
[36] Z. Zhang, K. Leinenweber, M. Bauer, L. A. J. Garvie, P. F. McMillan, G. H. Wolf, *J. Am. Chem. Soc.* **2001**, *123*, 7788-7796.
[37] P. F. McMillan, V. Lees, E. Quirico, G. Montagnac, A. Sella, B. Reynard, P. Simon, E. Bailey, M. Deifallah, F. Corà, *J. Solid State Chem.* **2009**, *182*, 2670-2677.
[38] E. Quirico, G. Montagnac, V. Lees, P. F. McMillan, C. Szopa, G. Cernogora, J. N. Rouzaud, P. Simon, J. M. Bernard, P. Coll, N. Fray, R. D. Minard, F. Raulin, B. Reynard, B. Schmitt, *Icarus* **2008**, *198*, 218-231.
[39] B. Jürgens, E. Irran, J. Senker, P. Kroll, H. Müller, W. Schnick, *J. Am. Chem. Soc.* **2003**, *125*, 10288-10300.
[40] A. E. Aliev, K. D. M. Harris, P. H. Champkin, *J. Phys. Chem. B* **2005**, *109*, 23342-23350.
[41] E. Wirnhier, M. Döblinger, D. Gunzelmann, J. Senker, B. V. Lotsch, W. Schnick, *Chem. Eur. J.* **2011**, *17*, 3213-3221.
[42] S. Y. Chong, J. T. A. Jones, Y. Z. Khimyak, A. I. Cooper, A. Thomas, M. Antonietti, M. J. Bojdys, *J. Mater. Chem. A* **2013**, *1*, 1102-1107.
[43] A. Zambon, J. M. Mouesca, C. Gheorghiu, P. A. Bayle, J. Pecaut, M. Claeys-Bruno, S. Gambarelli, L. Dubois, *Chem. Sci.* **2016**, *7*, 945-950.
[44] Z. Chen, P. Sun, B. Fan, Q. Liu, Z. Zhang, X. Fang, *Appl. Catal., B* **2015**, *170*, 10-16.
[45] Y. Hu, Y. Shim, J. Oh, S. Park, S. Park, Y. Ishii, *Chem. Mater.* **2017**, *29*, 5080-5089.
[46] J. Gracia, P. Kroll, *J. Mater. Chem.* **2009**, *19*, 3013-3019.
[47] R. Selvaraj, K. Qi, S. M. Z. Al-Kindy, M. Sillanpaa, Y. Kim, C.-W. Tai, *RSC Adv.* **2014**, *4*, 15371-15376.
[48] G. Marimuthu, M. Arivanandhan, C. Vedhi, *Synthesis and Reactivity in Inorganic, Metal-Organic, and Nano-Metal Chemistry* **2015**, *45*, 217-224.
[49] I. Galain, P. B. María, A. Ivana, F. Laura, *J. Cryst. Growth* **2017**, *457*, 227-233.

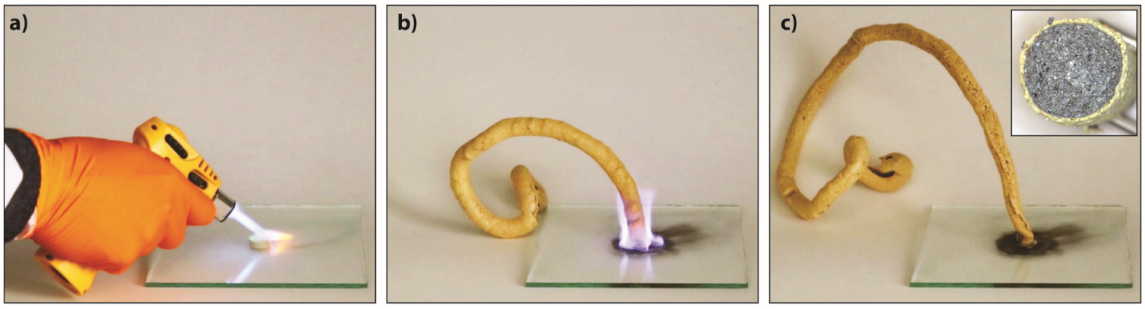

Figure 1: The Pharaoh's serpents formation reaction. Photographs showing the ignition of $Hg(SCN)_2$ (a), the progress of the self-propagating combustion reaction (b) and the final reaction product (c). Inset in (c) shows a cross section of one of the branches of the Pharaoh's serpent product material.

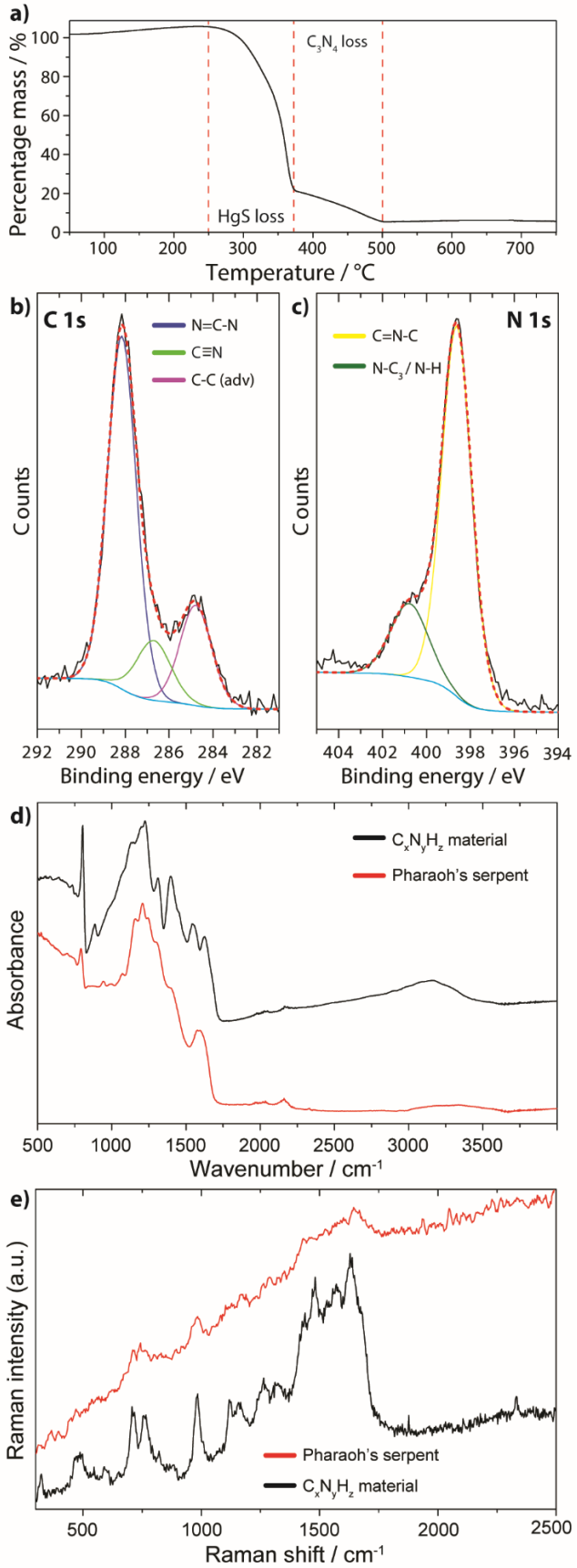

Figure 2. Thermogravimetric and spectroscopic analysis of the material produced by the Pharaoh's serpent reaction. a) TGA between 50 and 750 °C performed in flowing He. b) and c) C1s and N1s spectra of Pharaoh's serpent material (BE = Binding energy). d) ATR FTIR spectrum of Pharaoh's serpent C_3N_4 compared with polymeric-graphitic $C_xN_yH_z$ material synthesized by controlled thermal decomposition from melamine[22] (e) Raman spectra (325 nm laser excitation) of Pharaoh's serpent material compared with that of the $C_xN_yH_z$ polymeric solid.

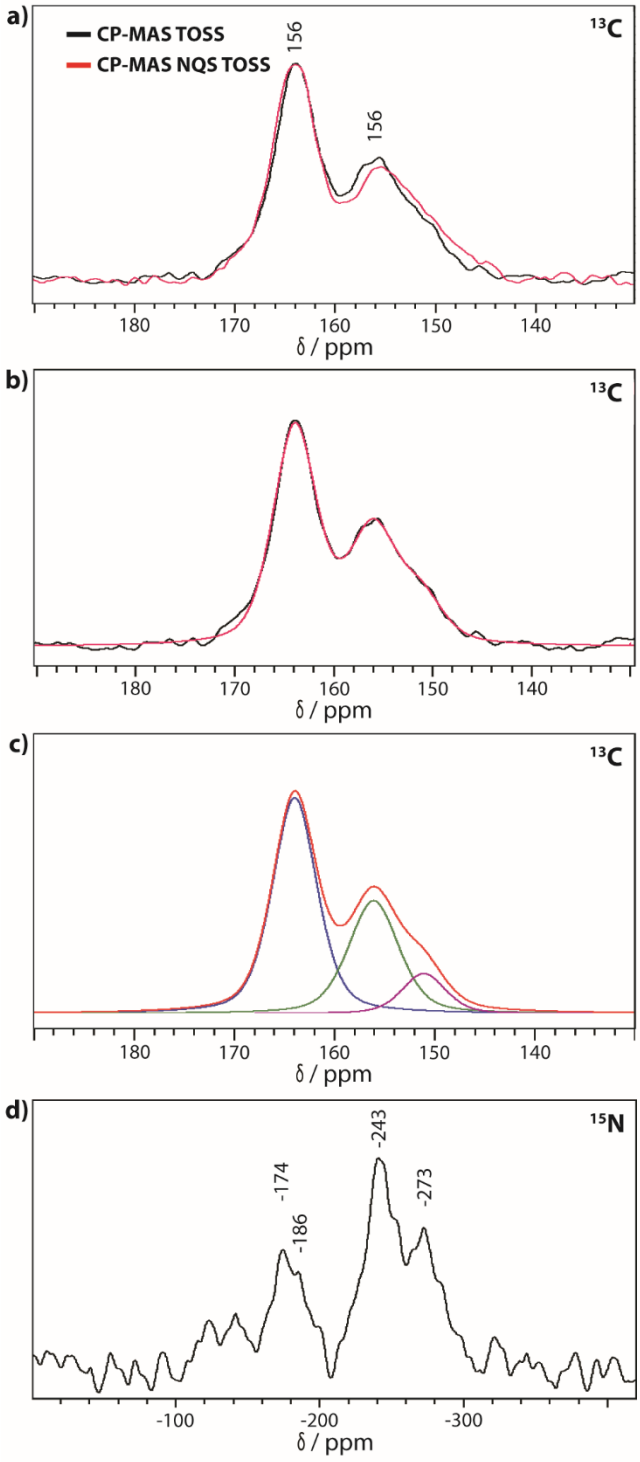

Figure 3: a) CP-MAS TOSS and NQS solid state ^{13}C NMR spectra of the C_3N_4 compound. b) The CP-MAS TOSS ^{13}C NMR spectrum of Pharaoh's serpent material (shown in black) fitted with the sum of three peaks (shown in red); c) Individual fitted peaks at 163.9, 156.0 and 151.0 ppm with the integral intensity ratio of 5.43:3.21:1.00 and the linewidths of 397, 448 and 391 Hz, respectively, together with their sum. d) The ^{15}N CP-MAS NMR spectrum of Pharaoh's serpent material.

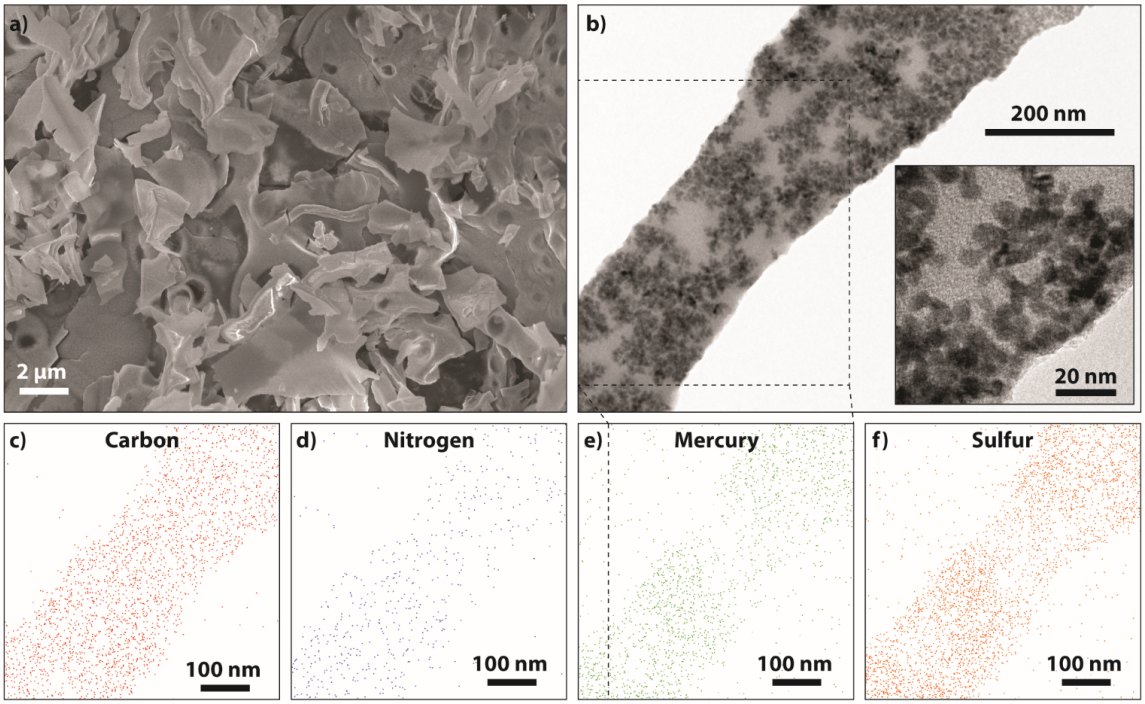

Figure 4: Micro- to nanoscale structure of Pharaoh's serpent material. SEM (a) and TEM (b) images of Pharaoh's serpent. EDS maps showing the distribution of carbon (c), nitrogen (d), mercury (e) and sulfur (f) in the suspended section of Pharaoh's serpent shown in (b).

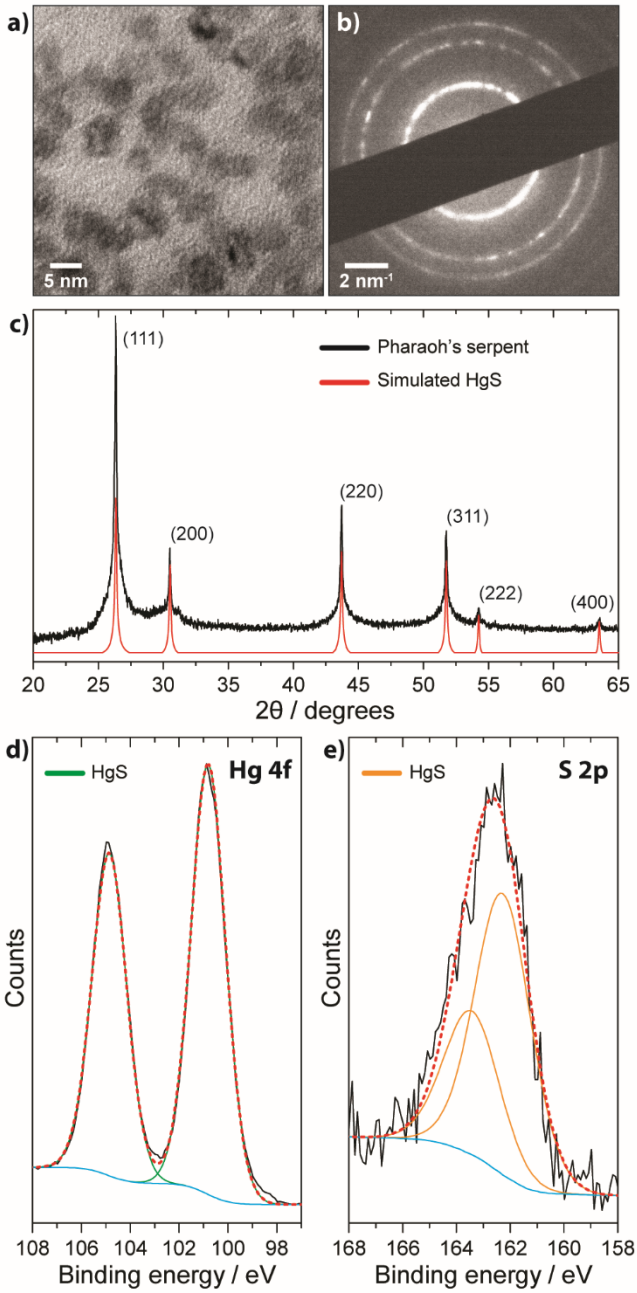

Figure 5: Characterization of HgS nanoparticles. TEM image (a) and electron diffraction pattern (b) of the HgS nanoparticles formed during the Pharaoh's serpents reaction. c) Powder XRD pattern (Cu Ka radiation) of Pharaoh's serpent overlaid with a simulated pattern for metacinnabar. XPS Hg 4f (d) and S 2p (e) spectra of Pharaoh's serpent.

Pharaoh's serpents: New insights into a classic carbon nitride material

Thomas S. Miller, Anita d'Aleo, Theo Suter, Abil E. Aliev, Andrea Sella, Paul F. McMillan

Supplementary movies

The supplementary movie M1 shows a real-time recording of the ignition and combustion of $Hg(SCN)_2$ in air to form a Pharaoh's serpent. Supplementary movie M2 shows this process being conducted in an N_2 atmosphere.

XPS

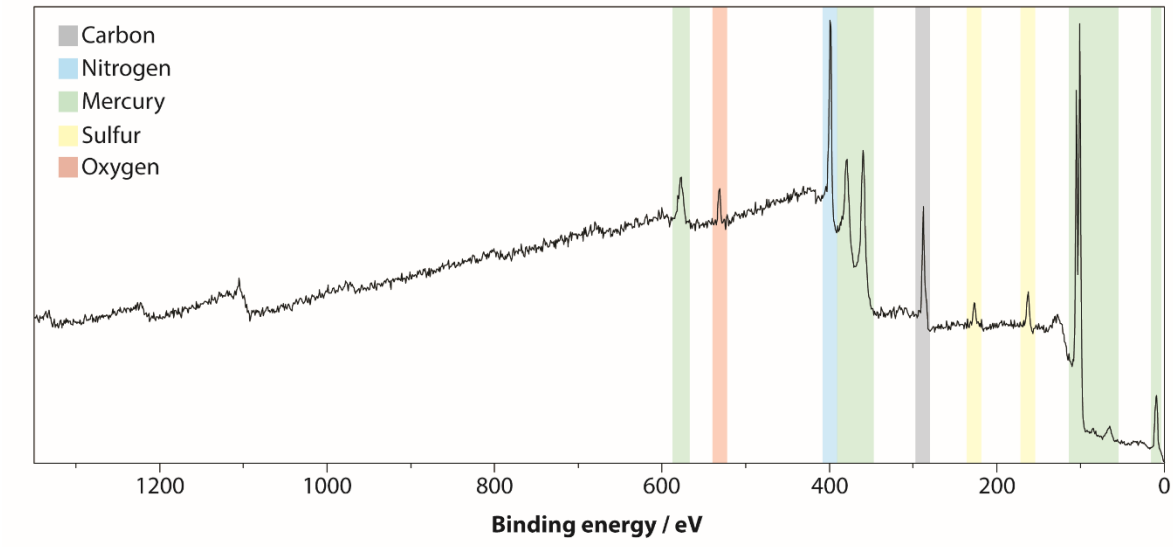

Figure S1: XPS survey spectrum of Pharaoh's serpent.

Element	Analysis (At %)
Carbon (incl. adventitious)	41.3
Nitrogen	42.3
Mercury	6.5
Sulfur	6.4

Oxygen	3.5

Table S1: Elemental composition of Pharaoh's serpent from XPS

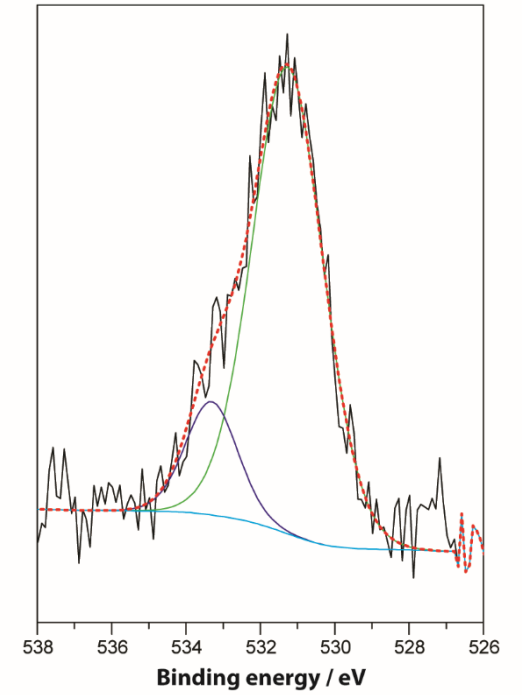

Figure S2: XPS of the O1s region measured for Pharaoh's serpent.

Solid-state NMR

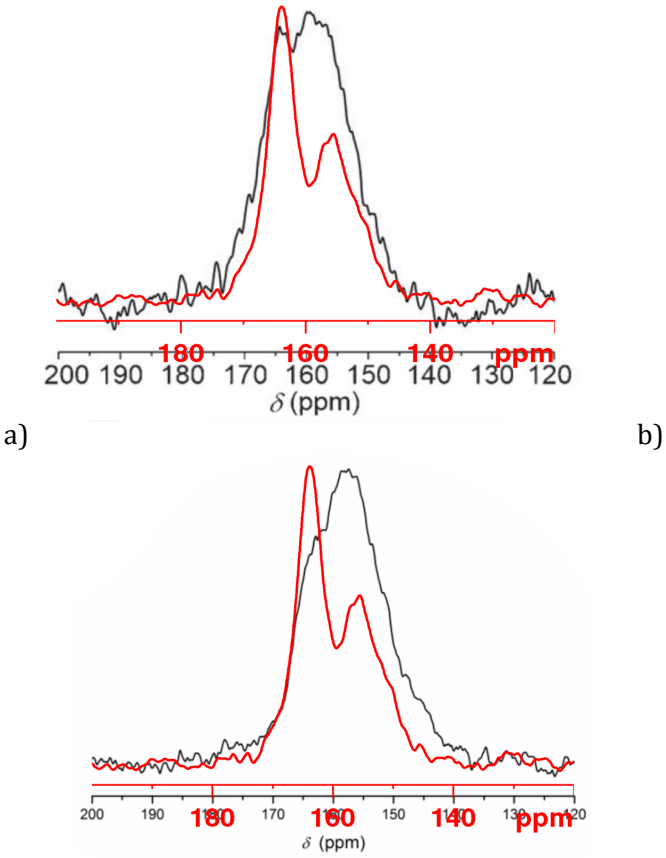

Figure S3: Overlaid view of the ^{13}C CP-MAS TOSS NMR spectrum of Pharaoh's serpent material (shown in red; magnetic field 7.05 T; MAS frequency 8 kHz; contact time 2 ms; recycle delay 5 s) with (a) the ^{13}C MAS NMR spectrum of triazine based graphitic carbon nitride, TGCN (shown in black; from reference [13] in the main text; magnetic field 9.4 T; MAS frequency 10 kHz) and (b) the ^{13}C CP-MAS TOSS NMR spectrum of TGCN (shown in black; from reference [13] in the main text; magnetic field 9.4 T; MAS frequency 10 kHz; contact time 2 ms; recycle delay 10 s). Reprinted with permission from ref. 13. Copyright John Wiley and Sons.

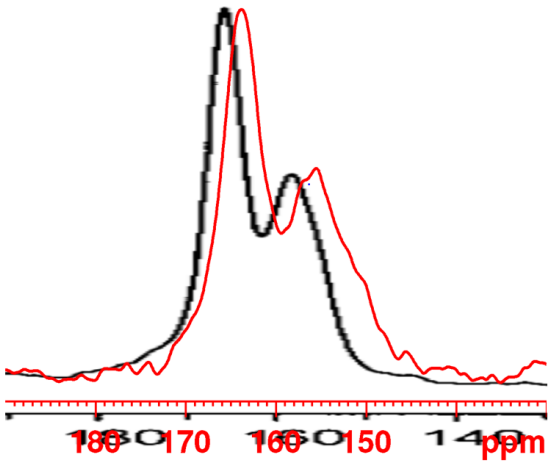

Figure S4: Overlaid view of the ^{13}C CP-MAS TOSS NMR spectrum of Pharaoh's serpent material (shown in red; magnetic field 7.05 T; MAS frequency 8 kHz; contact time 2 ms;

recycle delay 5 s with the ^{13}C CP-MAS NMR spectrum of poytriazine imide (PTI) $C_6N_9H_3 \cdot HCl$ (shown in black; from reference [36] in the main text; magnetic field 9.7 T; MAS frequency 9 kHz; contact time 3 ms; recycle delay 3 s). Reprinted (adapted) with permission from [36]. Copyright (2001) American Chemical Society.

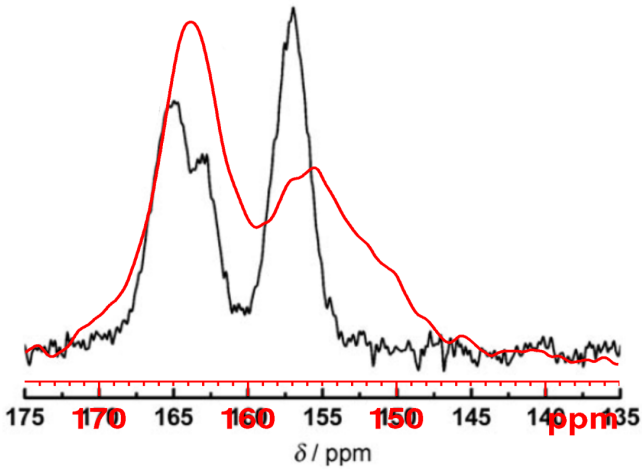

Figure S5: Overlaid view of the ^{13}C CP-MAS TOSS NMR spectrum of Pharaoh's serpent material (shown in red; magnetic field 7.05 T; MAS frequency 8 kHz; contact time 2 ms; recycle delay 5 s with the ^{13}C CP-MAS NMR spectrum of poly(aminoimino)heptazine, also known as Liebig's melon (shown in black; from reference [11] in the main text; the particular experimental details for this spectrum were not reported). Reprinted with permission from ref. 11. Copyright John Wiley and Sons.

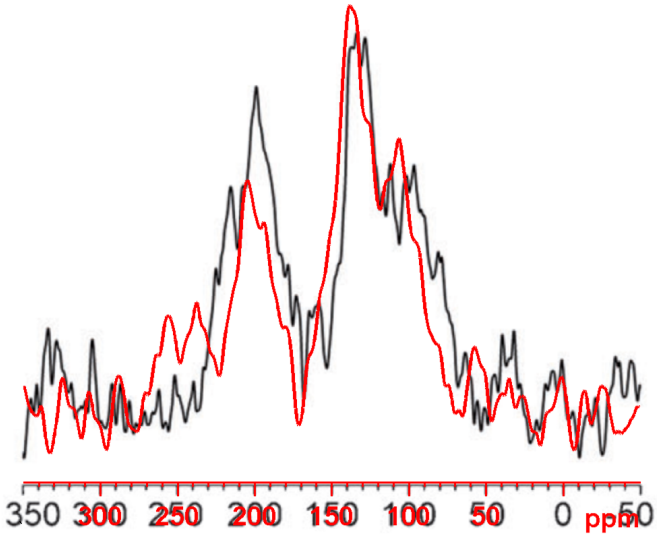

Figure S6: Overlaid view of ^{15}N CP-MAS NMR spectra of Pharaoh's serpent material (shown in red; magnetic field 7.05 T; MAS frequency 8 kHz; contact time 2 ms; recycle delay 5 s) and triazine based graphitic carbon nitride, TGCN (shown in black; from reference [13] in the main text; magnetic field 9.4 T; MAS frequency 5 kHz; contact time of 5 ms; recycle delay 10s). For consistency with reference [13] in the main text, ^{15}N spectra are referenced to the $-NH_2$ signal of glycine at 32.5 ppm with respect to liquid NH_3. The longer contact time of 5 ms used for TGCN is expected to enhance the relative intensity of non-protonated ^{15}N signals at ~200 ppm compared to those in the ^{15}N CP-

MAS NMR spectrum of Pharaoh's serpent material recorded with the contact time of 2 ms. Reprinted with permission from ref. 13. Copyright John Wiley and Sons.

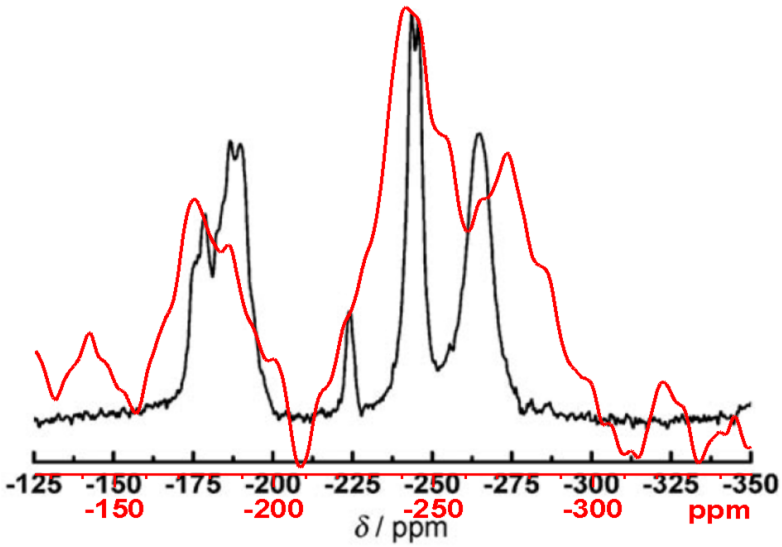

Figure S7: Overlaid view of ^{15}N CP-MAS NMR spectra of Pharaoh's serpent material (shown in red; magnetic field 7.05 T; MAS frequency 8 kHz; contact time 2 ms; recycle delay 5 s) and Liebig's melon (shown in black; from reference [11] in the main text; the particular experimental details for this spectrum were not reported). For consistency with reference [11] in the main text, ^{15}N spectra are referenced to the -NH_2 signal of glycine at -347.2 ppm with respect to nitromethane. Reprinted with permission from ref. 11. Copyright John Wiley and Sons. The latter was estimated using the ^{15}N NMR chemical shifts of glycine (33.4 ppm) and nitromethane (380.6 ppm) relative to liquid NH_3, as reported by Bertani et al. [P. Bertani, J. Raya, B. Bechinger, *Solid State NMR*, 2014, **61-61**, 15-18.]

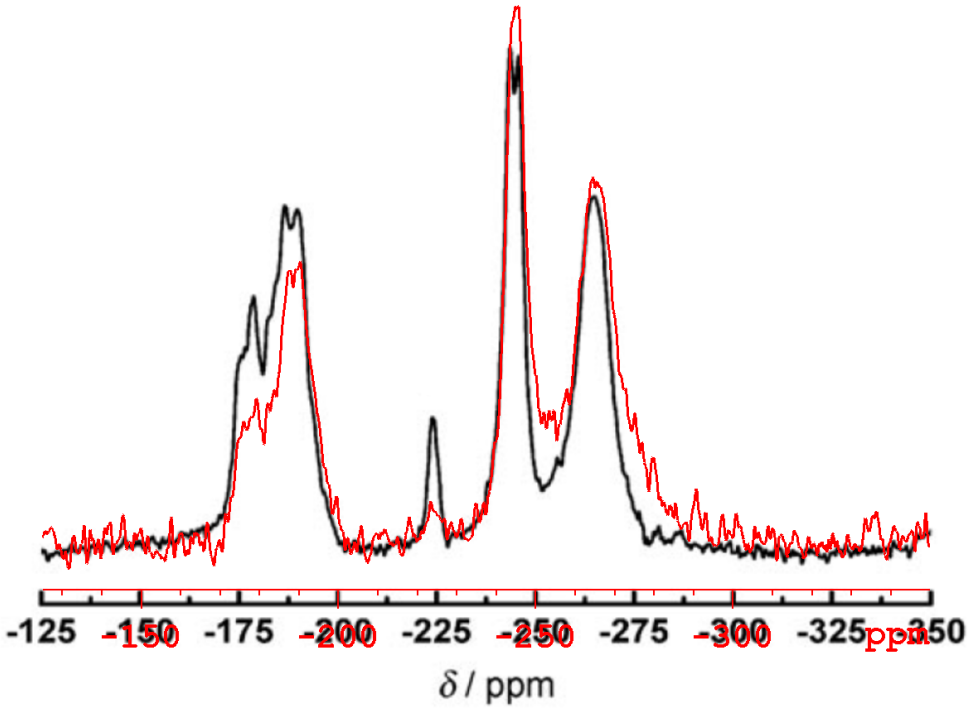

Figure S8: Overlaid view of the natural-abundance ^{15}N CP-MAS spectrum of the Liebig's melon using a short contact time of 1 ms (shown in red; magnetic field 7.05 T; MAS

frequency 4.8 kHz; recycle delay 4 s, total acquisition time 67 hours) with the ^{15}N CP-MAS NMR spectrum of ^{15}N-enriched Liebig's melon recorded using a contact time of either 10 or 20 ms (shown in black; from reference [11] in the main text; the particular experimental details for this spectrum were not reported). Reprinted with permission from ref. 11. Copyright John Wiley and Sons.

SEM

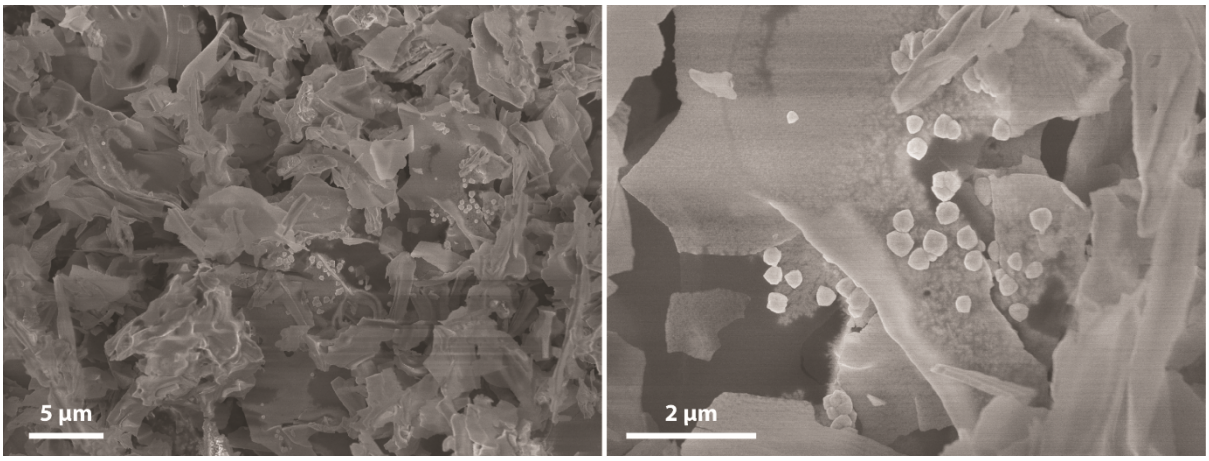

Figure S9: SEM images of Pharaoh's serpent showing examples of larger HgS particles

TEM

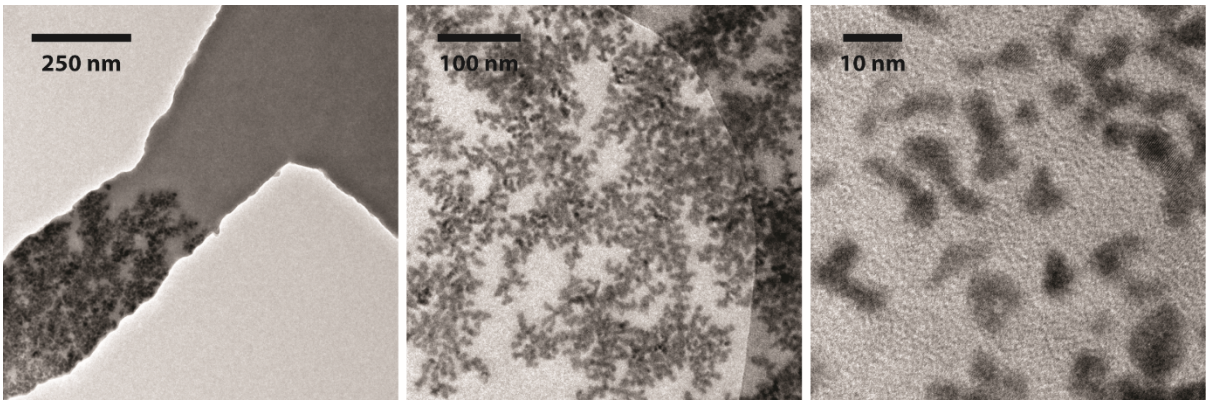

Figure S10: TEM images of Pharaoh's serpent showing HgS particles and areas of clear carbon nitride.

Crystal structure and simulated XRD

The CIF file for HgS was downloaded from the Inorganic crystal structure database at https://www.fiz-karlsruhe.de/icsd.html. *The structure is based on that reported by Rodic et al. [*D. Rodic, V. Spasojevic, A. Bajorek and P. Onnerud, *J. Magn. Magn. Mater.*, 1996, **152**, 159-164.] The predicted PXRD pattern of HgS was calculated using the 'powder pattern' function on the software 'Mercury' (Version 3.5.1).

ATR FTIR

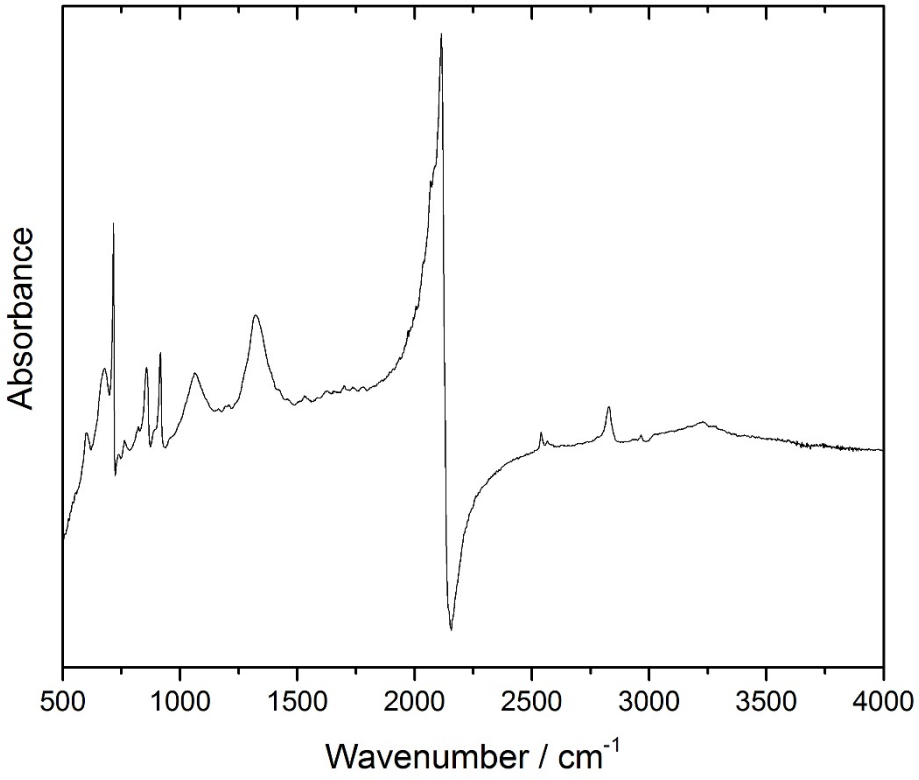

Figure S11: ATR FTIR spectrum of the $Hg(SCN)_2$ starting material. Note the unusual shape of the peaks is due to the fact that the spectrum is dominated by reflectance components. The main resonance at 2200 cm^{-1} is due to C≡N stretching within the SCN groups.